Research Inventy: International Journal of Engineering and Science
Vol.16, Issue 7 (July 2026), PP 54-64
Issn (e): 2278-4721, Issn (p):2319-6483, www.researchinventy.com

Robust Voltage Regulation of a Renewable-Integrated Single-Area Thermal Power System Using Neural-Network-Based Excitation Control

Nguyen Huu Thang*
Thanh Hoa College of Industry, Thanhhoa, Vietnam
Corresponding Author

ABSTRACT: *This paper develops a renewable-aware radial-basis-function neural-network (RBFNN) augmentation for terminal-voltage regulation of a small single-area thermal generating unit influenced by wind and photovoltaic power variations. The benchmark retains the dominant automatic-voltage-regulator amplifier, exciter, reduced generator-load voltage channel, first-order renewable channels, reactive-load disturbances, actuator saturation, controller memory, and parameter uncertainty. Four controllers are evaluated under identical operating conditions: PI, filtered PID, an explicit zero-order Takagi-Sugeno fuzzy-PI controller, and the proposed RBFNN controller. Unlike a rule-based compensation term, the proposed neural component is trained inside the supplied MATLAB script from 8000 deterministic excitation samples covering the load-renewable operating region and a ±25% plant-parameter family. Sixty-four Gaussian basis functions and ridge regression are used, and the learned output is bias-corrected to preserve the nominal equilibrium. Three nominal disturbance scenarios, a deterministic perturbed plant, and twenty deterministic quasi-random ±25% parameter realizations are examined. Relative to PID, the RBFNN reduces IAE by 54.2%, 66.2%, and 70.2% in the three nominal cases. In the severe perturbed case, IAE and RMS voltage deviation decrease by 59.4% and 53.5%, respectively. Across the twenty-plant robustness ensemble, mean IAE falls from 0.1569 to 0.0531 p.u.·s, a reduction of 66.2%, while mean control effort rises by only 5.5%. A local Lyapunov analysis based on the actual trained RBF gradient yields a Hurwitz closed-loop matrix, a positive-definite Lyapunov matrix, and a residual of 1.88e-13. The results show that a compact, deterministically trained neural augmentation can improve disturbance rejection and parameter robustness while retaining a transparent excitation-control structure.*

Keywords: *automatic voltage regulator; excitation control; radial-basis-function neural network; fuzzy logic; thermal generating unit; wind power; photovoltaic generation; Lyapunov stability; robust voltage control.*

Date of Submission: 06-07-2026 Date of Acceptance: 17-07-2026

NOMENCLATURE

Symbol	Description	Unit
$V_t, \Delta V_t$	Terminal voltage and terminal-voltage deviation	p.u.
V_a	AVR amplifier state	p.u.
E_{fd}	Exciter field-voltage state	p.u.
ΔQ_L	Reactive-load disturbance	p.u.
q_W, q_{PV}	Filtered wind and photovoltaic voltage-support channels	p.u.
K_A, T_A	Amplifier gain and time constant	-, s
K_E, T_E	Exciter gain and time constant	-, s
K_G, T_G	Generator-load gain and time constant	-, s
K_L, K_W, K_{PV}	Reactive-load, wind, and PV coupling coefficients	-
u_c	Excitation control command	p.u.
e	Terminal-voltage regulation error	p.u.
ξ	Integral state of the voltage error	p.u.·s
d_f	Filtered derivative of voltage error	p.u./s
ϕ_j	Output of the jth Gaussian RBF neuron	-
w	RBF output-weight vector	-
IAE, ITAE	Integral absolute and time-weighted absolute errors	p.u.·s, p.u.·s²

I. INTRODUCTION

Voltage regulation is a core dynamic-control task of synchronous generating units. Excitation control must maintain terminal voltage, support reactive-power balance, and interact safely with the wider plant and grid. Contemporary stability definitions, excitation-system modeling recommendations, distributed-energy interconnection requirements, and transmission-level inverter-based-resource requirements provide the formal context for such studies [1]-[4]. Modern power-system texts further emphasize that voltage response depends on excitation dynamics, network strength, reactive-power balance, controller bandwidth, operating point, and model fidelity [5].

The operating environment is changing. Wind and photovoltaic plants are converter-interfaced, and their short-term behavior is shaped by software, current limits, grid-following or grid-forming control, plant-level coordination, and interconnection rules. Recent work and official roadmaps document the associated low-inertia and inverter-dominated stability challenges [6]-[13]. These sources do not imply that every renewable variation directly drives generator terminal voltage. Rather, they motivate explicit testing of voltage controllers against changing renewable-mediated reactive-power conditions and parameter uncertainty.

Data-driven voltage regulation has progressed rapidly. Recent studies include machine-learning-assisted local control, ancillary-service coordination, sensitivity learning, input-convex networks, deep reinforcement learning, robust Volt/VAr control, self-adaptive droop design, stability-constrained smart-inverter rules, and scalable multi-agent coordination [14]-[33]. The common lesson is not that learning automatically guarantees better control. It is that measured operating context can improve decisions when the learned mapping is trained over a representative domain and embedded inside a structure with explicit limits.

Learning-assisted power-system optimization and stability assessment have also been reviewed systematically [34]-[36]. Neural voltage-control applications, neural predictive control, adaptive fuzzy excitation control, AVR tuning, and stability-preserving PID learning provide related evidence that nonlinear data-driven policies can complement classical feedback rather than merely replace it [37]-[43]. General learning references and recent work on verification and neural Lyapunov methods highlight a second requirement: performance claims should be separated from stability claims, and the validity domain of any proof should be stated explicitly [44]-[52].

This study therefore asks a narrow, reproducible question: *Can a genuinely trained renewable-aware RBF neural augmentation improve excitation-based terminal-voltage regulation of a small thermal generating unit when load, wind, PV, and plant uncertainty act simultaneously?* The paper makes five contributions. First, it states the reduced-order modeling scope and its limitations explicitly. Second, it implements a genuine RBF training stage using 8000 deterministic samples spanning both operating context and a ±25% parameter family. Third, it compares PI, filtered PID, explicit zero-order Takagi-Sugeno fuzzy-PI, and RBFNN control under identical limits and disturbance scenarios. Fourth, it evaluates a deterministic perturbed plant and twenty deterministic quasi-random parameter realizations. Fifth, it derives a local Lyapunov certificate from the actual trained-network gradient rather than from nominal hand-selected neural gains.

The benchmark is intentionally not a substitute for a full electromagnetic-transient or network-level voltage-security study. Boiler-turbine and active-power speed loops are outside the short terminal-voltage timescale represented here. The wind and PV channels represent converter-mediated voltage-support influence at the point of coupling; they are not detailed switching models. This scope is sufficient for a controlled comparison of excitation strategies, but field deployment would require substantially richer validation.

II. MATHEMATICAL MODEL OF THE RENEWABLE-ASSISTED THERMAL VOLTAGE CHANNEL

A. AVR amplifier and exciter

The supplementary controller drives a first-order AVR amplifier:

$$T_A \dot{V}_a = -V_a + K_A u_c. \qquad (1)$$

The exciter is represented by

$$T_E \dot{E}_{fd} = -E_{fd} + K_E V_a. \qquad (2)$$

These equations retain the dominant short-term lag between controller command and field excitation, consistent with the reduced-order comparison objective and the modeling discipline encouraged by excitation-system practice [2].

B. Reduced generator-load voltage channel

Let $\Delta V_t = V_t - V_{t0}$ denote terminal-voltage deviation around the initial operating point. The reduced generator-load channel is

$$T_G \Delta\dot{V}_t = -\Delta V_t + K_G E_{fd} - K_L \Delta Q_L + K_W q_W + K_{PV} q_{PV}. \qquad (3)$$

Here ΔQ_L is a reactive-load disturbance. The terms q_W and q_{PV} are filtered converter-mediated voltage-support channels. Positive renewable terms are defined as voltage supporting under the adopted small-signal sign convention.

The wind and PV channels obey

$$T_W \dot{q}_W = -q_W + q_W^{\star}(t), \quad (4)$$
$$T_{PV} \dot{q}_{PV} = -q_{PV} + q_{PV}^{\star}(t). \quad (5)$$

The state vector is

$$x = [V_a \quad E_{fd} \quad \Delta V_t \quad q_W \quad q_{PV}]^T. \quad (6)$$

Accordingly, the benchmark can be written as

$$\dot{x} = f(x, u_c, \Delta Q_L, q_W^{\star}, q_{PV}^{\star}; \theta), \quad (7)$$

where θ collects the eleven gains and time constants listed in Table 1.

Table 1. Nominal parameters of the reduced-order benchmark.

Parameter	Symbol	Nominal value	Unit
Amplifier gain	K_A	10.0	-
Amplifier time constant	T_A	0.1	s
Exciter gain	K_E	1.0	-
Exciter time constant	T_E	0.4	s
Generator-load gain	K_G	1.0	-
Generator-load time constant	T_G	1.0	s
Reactive-load coefficient	K_L	0.9	-
Wind coupling coefficient	K_W	0.6	-
PV coupling coefficient	K_{PV}	0.65	-
Wind channel time constant	T_W	0.5	s
PV channel time constant	T_{PV}	0.35	s

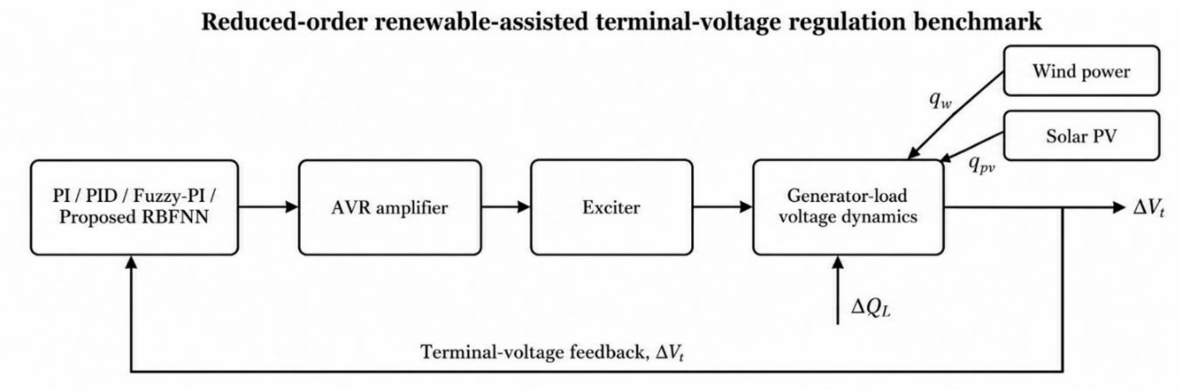

Fig. 1. Reduced-order architecture used for the controller comparison.

C. Modeling scope and uncertainty family

The nominal model is used for controller comparison, whereas robustness is probed through simultaneous parameter changes. For each uncertain parameter θ_i,

$$\theta_i = \rho_i \theta_{i0}, \qquad \rho_i \in [0.75, 1.25]. \quad (8)$$

The deterministic perturbed plant changes several gains and time constants in an adverse direction. The twenty-plant robustness ensemble uses deterministic quasi-random factors within the same interval. This removes run-to-run randomness from the supplied script while still sampling multiple directions in the parameter space.

III. CONTROL METHODOLOGIES

A. Common feedback variables

The voltage error is defined by

$$e(t) = \Delta V_t^{\star} - \Delta V_t(t), \qquad \Delta V_t^{\star} = 0. \qquad (9)$$

The integral state satisfies

$$\dot{\xi} = e, \quad (10)$$

with numerical clamping in $[-1,1]$ to prevent uncontrolled integral growth. A filtered derivative is used instead of an ideal differentiator:

$$T_f \dot{d}_f + d_f = \dot{e}. \quad (11)$$

B. PI and filtered PID baselines

The PI command is

$$u_{PI} = K_p e + K_i \xi. \qquad (12)$$

The filtered PID command is

$$u_{PID} = K_p e + K_i \xi + K_d d_f. \qquad (13)$$

Fixed gains are selected once and then held constant across all scenarios. This provides a transparent baseline and avoids retuning each controller for individual disturbances. Recent AVR reviews and stability-preserving tuning studies illustrate why gain selection and stability supervision remain important even for apparently simple PID structures [42], [43].

C. Explicit zero-order Takagi-Sugeno fuzzy-PI controller

The fuzzy benchmark is implemented explicitly, without the Fuzzy Logic Toolbox. Error and filtered derivative are normalized as

$$r_e = \mathrm{sat}\left(\frac{e}{0.08}, -1{,}1\right), \qquad r_d = \mathrm{sat}\left(\frac{d_f}{0.10}, -1{,}1\right). \qquad (14)$$

For each normalized input, three triangular membership grades are used:

$$\mu_N(r) = \max(-r, 0), \quad \mu_Z(r) = \max(1 - |r|, 0), \quad \mu_P(r) = \max(r, 0). \qquad (15)$$

The product-rule firing strength is

$$\omega_{ij} = \mu_i(r_e)\mu_j(r_d), \qquad i, j \in \{N, Z, P\}. \qquad (16)$$

Two 3×3 zero-order rule tables produce gain multipliers. Their weighted averages are

$$m_p = \frac{\sum_{i,j} \omega_{ij} g_{ij}^p}{\sum_{i,j} \omega_{ij}}, \qquad m_i = \frac{\sum_{i,j} \omega_{ij} g_{ij}^i}{\sum_{i,j} \omega_{ij}}. \qquad (17)$$

The command is

$$u_{FPI} = 0.45 m_p e + 0.22 m_i \xi. \qquad (18)$$

This is a genuine fuzzy inference benchmark rather than a heuristic nonlinear gain schedule. Adaptive fuzzy excitation control has been demonstrated in related synchronous-generator studies [41].

D. Proposed renewable-aware RBF neural augmentation

The proposed context vector is

$$z = [e \quad d_f \quad \Delta Q_L \quad q_W \quad q_{PV}]^T. \qquad (19)$$

Each feature is normalized by a fixed scale vector s:

$$\bar{z}_i = \frac{z_i}{s_i}, \qquad s = [0.08 \quad 0.18 \quad 0.15 \quad 0.07 \quad 0.08]^T. \qquad (20)$$

For center c_j and common width σ, the jth Gaussian basis is

$$\phi_j(\bar{z}) = \exp\left[-\frac{\|\bar{z} - c_j\|_2^2}{2\sigma^2}\right], \qquad j = 1, \ldots, 64. \quad (21)$$

Training uses $N = 8000$ deterministic samples. Eleven irrational multipliers generate repeatable low-discrepancy-like excitation coordinates, which are mapped into the specified error, derivative, load, renewable, and ±25% parameter ranges. The supervised target is

$$y = 0.012\tanh(30e) + 0.004\tanh(25d_f) + \frac{K_L \Delta Q_L - K_W q_W - K_{PV} q_{PV}}{K_A K_E K_G}. \qquad (22)$$

The first two terms provide smooth nonlinear error shaping. The last term teaches a context compensation consistent with the reduced voltage equation. Because the target is generated over a parameter family rather than only the nominal plant, the learned map is not simply a lookup table for one fixed model.

The output weights solve the regularized least-squares problem

$$\min_w \ \| \Phi w - y \|_2^2 + \lambda \| w \|_2^2, \qquad (23)$$

with closed-form solution

$$w = (\Phi^T \Phi + \lambda R)^{-1} \Phi^T y, \quad (24)$$

where the bias entry is not regularized. The raw network output is

$$u_{NN}^{raw} = w_0 + \sum_{j=1}^{64} w_j \, \phi_j(\bar{z}). \qquad (25)$$

To preserve the nominal zero-disturbance equilibrium, the output at the origin is removed:

$$u_{NN}(z) = u_{NN}^{raw}(z) - u_{NN}^{raw}(0). \qquad (26)$$

The proposed command is

$$u_{RBF} = 0.70e + 0.30\xi + 0.06d_f + u_{NN}(z). \quad (27)$$

Finally, every controller is subjected to the same actuator limit:

$$u_c = \mathrm{sat}(u, -0.5{,}0.5). \qquad (28)$$

The architecture is shown in Fig. 2. Related neural voltage-control and neural predictive-control studies support the broader use of learned nonlinear mappings in energy-conversion control [37]-[40], while [44] provides general neural-learning foundations.

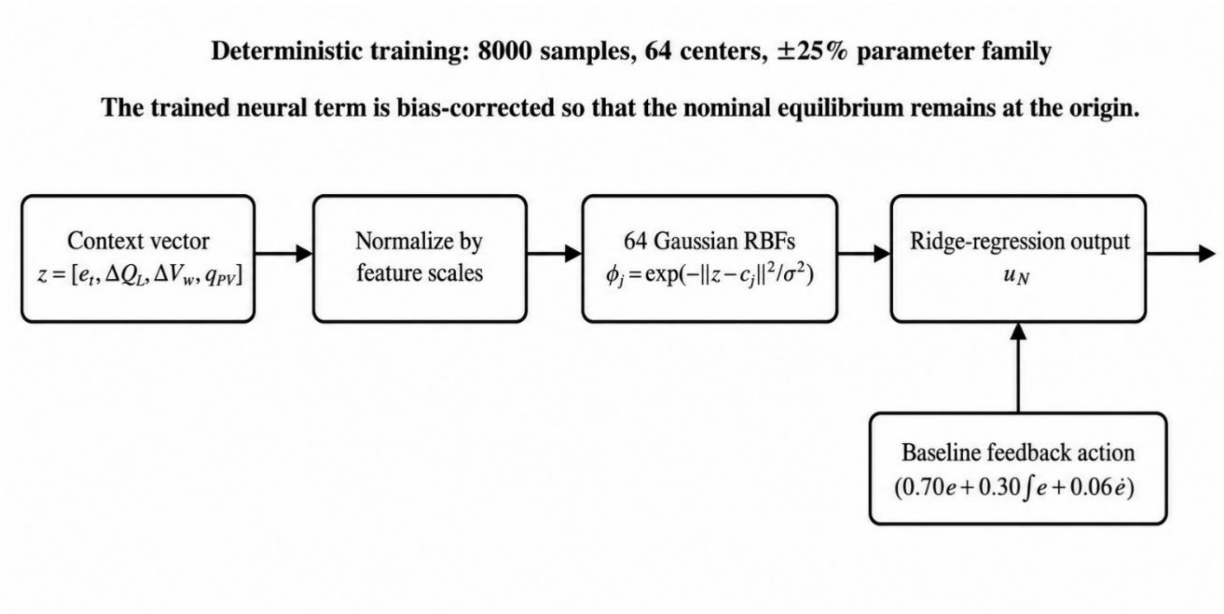

Fig. 2. Structure and deterministic training principle of the proposed RBFNN augmentation.

Table 2. Trained RBFNN summary reproduced by the reference model.

Quantity	Value
Training samples	8000
Gaussian neurons	64
Common width σ	0.864741
Training RMSE	0.002960
Training MAE	0.002153
Removed origin bias	1.038282e-04

IV. LOCAL STABILITY ANALYSIS USING A LYAPUNOV FUNCTION

The nonlinear closed loop contains saturation and a trained RBF map. A global proof is not claimed. Instead, the analysis is local, nominal, unsaturated, and disturbance free. This distinction is important because recent neural-control literature explicitly separates empirical performance from formal stability certification [48], [51], [52].

Define the local augmented state

$$x_a = [V_a \quad E_{fd} \quad \Delta V_t \quad \xi \quad d_f]^T. \quad (29)$$

The actual trained RBF gradient at $z = 0$ is used to obtain effective local gains:

$$K_e = 0.70 + \left.\frac{\partial u_{NN}}{\partial e}\right|_0, \qquad K_i = 0.30, \qquad K_d = 0.06 + \left.\frac{\partial u_{NN}}{\partial d_f}\right|_0. \qquad (30)$$

The local model is

$$\dot{x}_a = A_{cl} x_a. \quad (31)$$

For the implemented derivative filter, the closed-loop matrix is

$$A_{cl} = \begin{bmatrix} -1/T_A & 0 & -K_A K_e/T_A & K_A K_i/T_A & K_A K_d/T_A \\ K_E/T_E & -1/T_E & 0 & 0 & 0 \\ 0 & K_G/T_G & -1/T_G & 0 & 0 \\ 0 & 0 & -1 & 0 & 0 \\ 0 & -K_G/(T_f T_G) & 1/(T_f T_G) & 0 & -1/T_f \end{bmatrix}. \quad (32)$$

For any $Q = Q^T > 0$, if A_{cl} is Hurwitz, the continuous Lyapunov equation

$$A_{cl}^T P + P A_{cl} = -Q \quad (33)$$

has a unique $P = P^T > 0$. With

$$V(x_a) = x_a^T P x_a, \quad (34)$$

its derivative is

$$\dot{V} = -x_a^T Q x_a < 0, \qquad x_a \neq 0. \quad (35)$$

The resulting eigenvalues are -22.5444, -7.0832, -1.7896 ± j5.3695, -0.2932. The largest real part is -0.293227. The smallest eigenvalue of P is 0.020932>0, and the Frobenius residual $\| A_{cl}^T P + P A_{cl} + Q \|_F$ is 1.883e-13. These checks establish local asymptotic stability of the nominal zero-disturbance equilibrium within the unsaturated neighborhood represented by the linearization. They do not establish global stability under arbitrary renewable disturbances, parameter shifts, or sustained saturation.

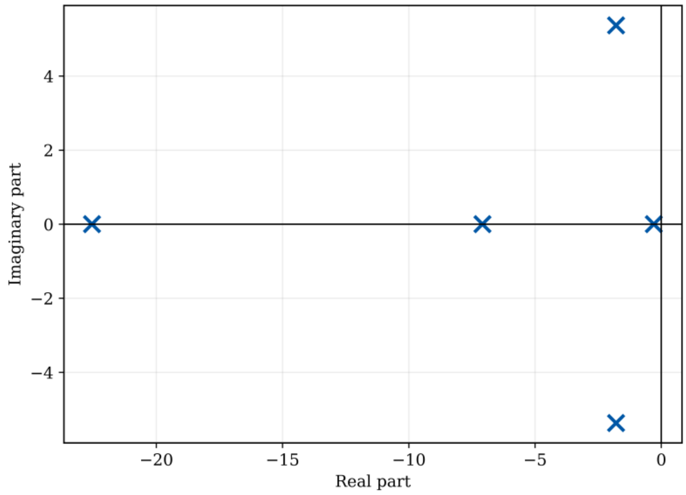

Fig. 10. Closed-loop eigenvalues of the locally linearized proposed controller.

V. SIMULATION DESIGN AND EXECUTION

All simulations use $\Delta t = 0.005$ s and a 50 s horizon. Scenario 1 combines coordinated steps in reactive load, wind support, and PV support. Scenario 2 uses continuously varying sinusoidal and cloud-like renewable profiles. Scenario 3 combines larger load changes, multi-frequency wind variation, and two pronounced PV events. Figure 3 shows the severe-case forcing profile.

The performance indices are

$$\mathrm{IAE} = \int_0^T |\Delta V_t(t)| \, dt, \quad (36)$$

$$\mathrm{ITAE} = \int_0^T t \, |\Delta V_t(t)| \, dt, \quad (37)$$

$$\mathrm{RMS} = \sqrt{\frac{1}{N} \sum_{k=1}^{N} \Delta V_t^2(k)}, \quad (38)$$

$$V_{pk} = \max_t |\Delta V_t(t)|, \quad (39)$$

$$J_u = \int_0^T u_c^2(t) \, dt. (40)$$

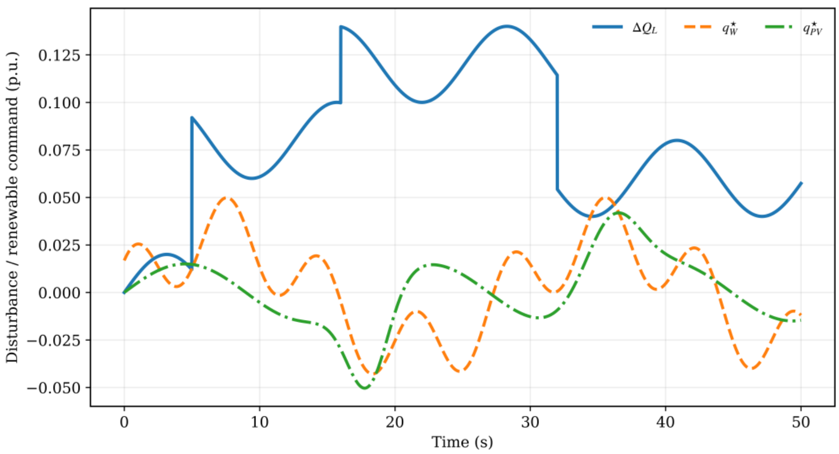

Fig. 3. Severe mixed-disturbance profiles used for Scenario 3.

A. Scenario 1: coordinated step disturbances

Figure 4 shows the nominal step-disturbance response. PID improves over PI, reducing IAE from 0.049045 to 0.042851 p.u.·s. The explicit Fuzzy-PI gives IAE = 0.047974 p.u.·s. The proposed RBFNN reaches 0.019643 p.u.·s, which is 54.2% below PID. RMS and peak deviation fall by 48.0% and 38.7%, respectively. The improvement is achieved with a modest increase in control effort from 0.001396 to 0.001488.

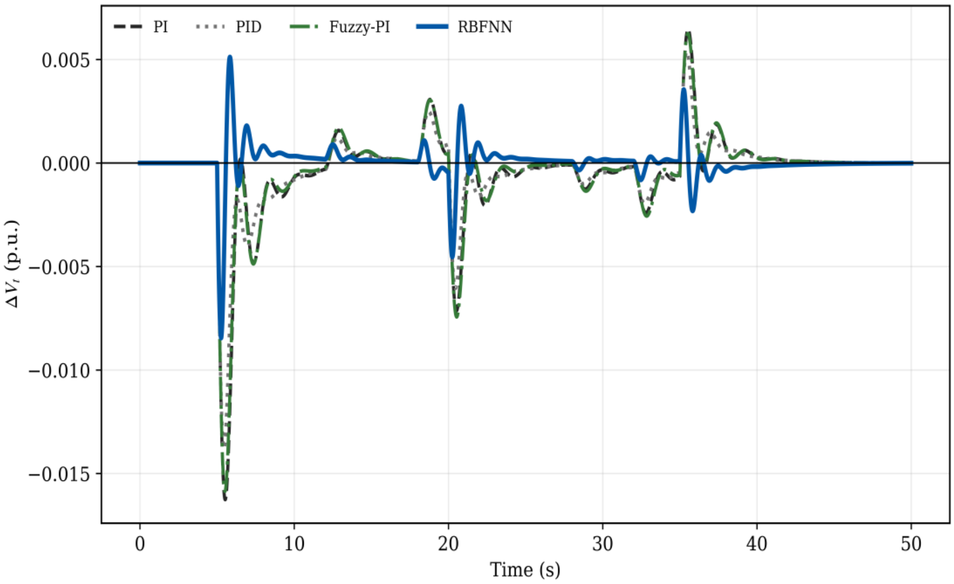

Fig. 4. Terminal-voltage response for Scenario 1.

B. Scenario 2: continuously varying wind, PV, and load

Scenario 2 removes long settling intervals and repeatedly changes the renewable context. PID produces IAE = 0.064793 p.u.·s and RMS = 0.001742 p.u. RBFNN reduces these values to 0.021899 p.u.·s and 0.000702 p.u. The corresponding improvements are 66.2% and 59.7%. This case is particularly informative because the learned context term can respond before integral action accumulates a large bias.

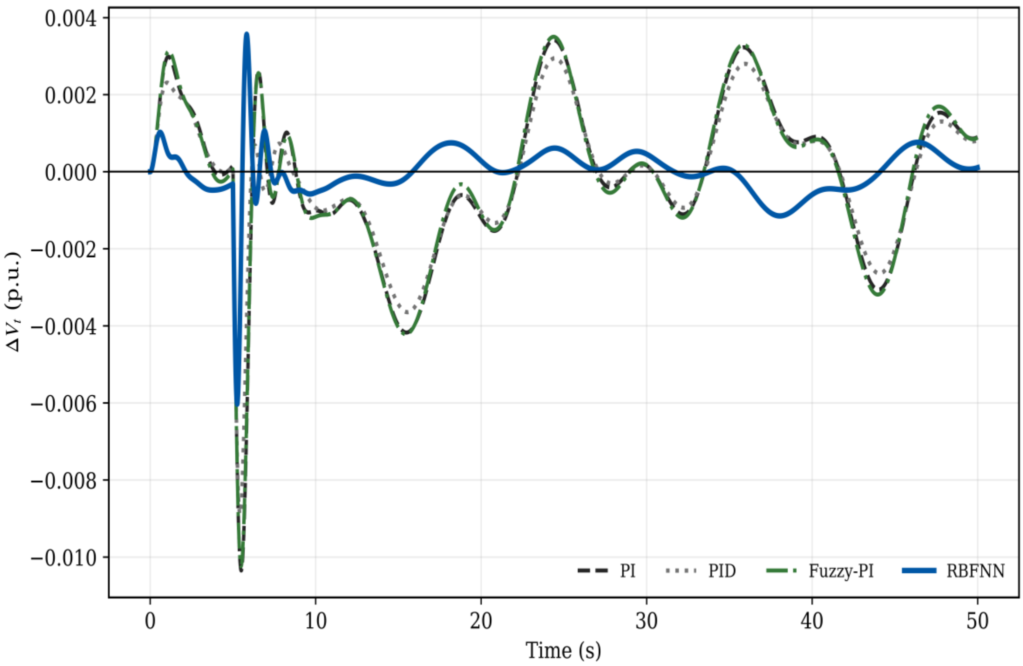

Fig. 5. Terminal-voltage response for Scenario 2.

C. Scenario 3: severe mixed disturbance

In Scenario 3, the nominal plant experiences larger load changes, multi-frequency wind variation, and pronounced PV events. All four controllers remain bounded. Their IAEs are 0.165446, 0.140546, 0.165029, and 0.041844 p.u.·s for PI, PID, Fuzzy-PI, and RBFNN, respectively. Relative to PID, the proposed method reduces IAE by 70.2%, RMS by 61.6%, and peak voltage deviation by 35.1%.

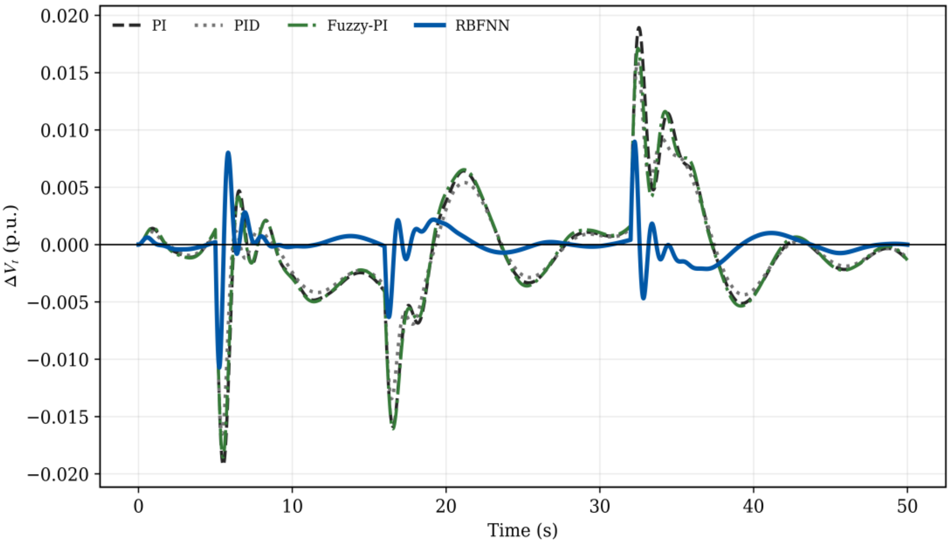

Fig. 6. Terminal-voltage response for Scenario 3.

Table 3. Nominal performance metrics for all scenarios.

Scenario	Controller	IAE (p.u.·s)	ITAE (p.u.·s²)	RMS (p.u.)	Peak (p.u.)	J_u
S1	PI	0.049045	0.896139	0.002265	0.016263	0.001396
S1	PID	0.042851	0.781040	0.001849	0.013795	0.001396
S1	Fuzzy-PI	0.047974	0.877591	0.002228	0.015860	0.001397
S1	**RBFNN**	**0.019643**	**0.366334**	**0.000961**	**0.008455**	0.001488
S2	PI	0.076277	1.781967	0.002055	0.010351	0.000461
S2	PID	0.064793	1.545025	0.001742	0.008890	0.000460
S2	Fuzzy-PI	0.076734	1.808437	0.002068	0.010237	0.000462
S2	**RBFNN**	**0.021899**	**0.501400**	**0.000702**	**0.006033**	0.000494
S3	PI	0.165446	3.946579	0.004872	0.019247	0.003478
S3	PID	0.140546	3.429968	0.004132	0.016537	0.003474
S3	Fuzzy-PI	0.165029	3.936524	0.004767	0.018546	0.003483
S3	**RBFNN**	**0.041844**	**0.966068**	**0.001588**	**0.010726**	0.003698

D. Deterministic perturbed plant

The perturbed plant simultaneously changes amplifier, exciter, generator-load, renewable-channel, and disturbance-coupling parameters. Figure 7 shows the severe-case response. PID yields IAE = 0.281511 p.u.·s, RMS = 0.008212 p.u., and peak deviation = 0.027255 p.u. RBFNN gives 0.114400 p.u.·s, 0.003821 p.u., and 0.017934 p.u., corresponding to reductions of 59.4%, 53.5%, and 34.2%. The result supports robustness of the learned augmentation within the tested family, but it is not a formal robust-stability proof.

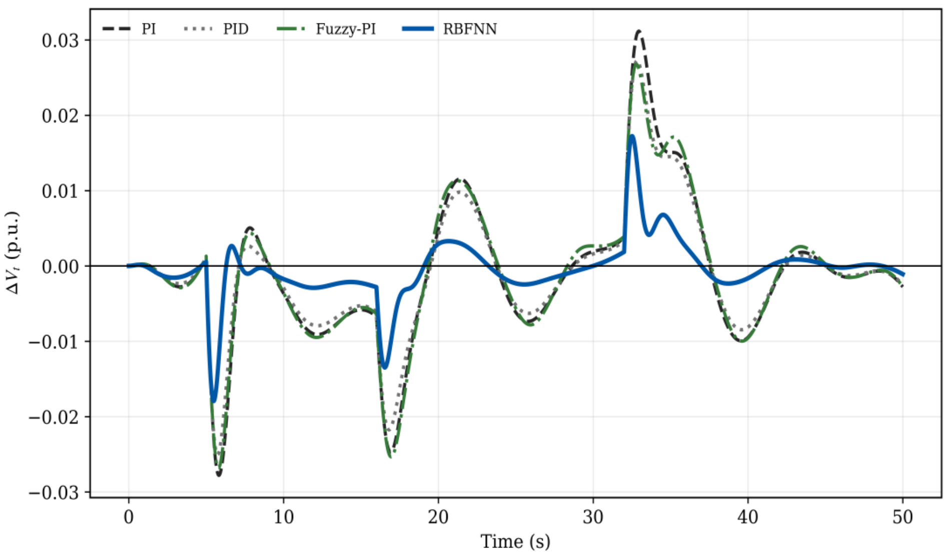

Fig. 7. Severe mixed disturbance for the deterministic perturbed plant.

Table 4. Severe perturbed-case results.

Controller	IAE	ITAE	RMS	Peak	Control effort
PI	0.326223	7.741303	0.009440	0.031158	0.018311
PID	0.281511	6.721618	0.008212	0.027255	0.018315
Fuzzy-PI	0.323457	7.649743	0.009106	0.026818	0.018319
RBFNN	**0.114400**	**2.533385**	**0.003821**	**0.017934**	0.018780

E. Aggregate and twenty-plant robustness comparison

Figure 8 compares IAE in all three nominal scenarios. RBFNN is consistently lower than PI, PID, and Fuzzy-PI. Figure 9 extends the comparison to twenty deterministic quasi-random parameter realizations. Mean IAE values are 0.183344, 0.156883, 0.182720, and 0.053051 p.u.·s. Thus, the neural controller improves mean IAE by 66.2% relative to PID. Mean RMS is reduced by 59.4%. Mean control effort increases by 5.5%, which is materially smaller than the error reduction.

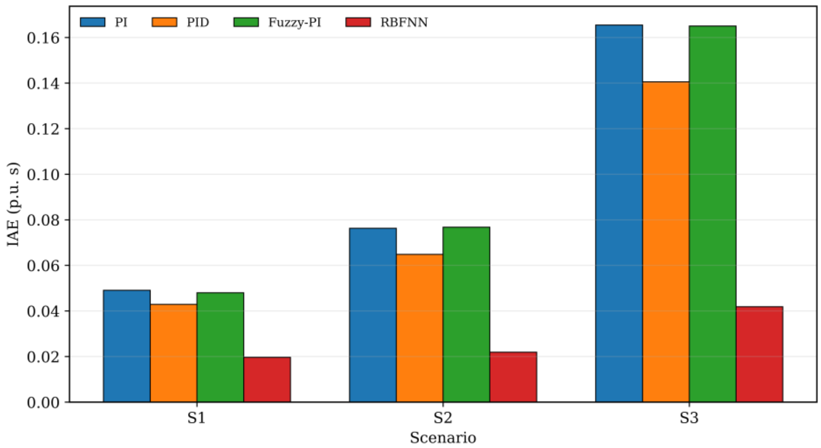

Fig. 8. IAE comparison across the three nominal scenarios.

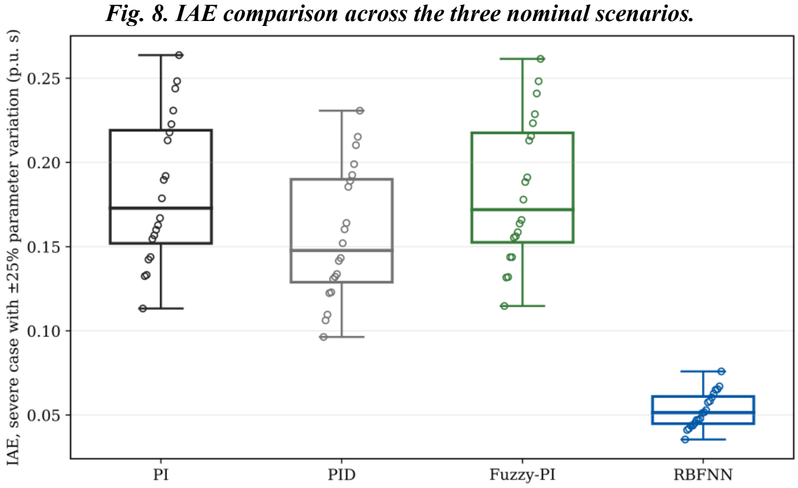

Fig. 9. IAE distribution over twenty deterministic ±25% parameter realizations.

Table 5. Mean metrics over twenty severe-case parameter realizations.

Controller	Mean IAE	Mean RMS	Mean peak	Mean control effort
PI	0.183344	0.005372	0.020208	0.004650
PID	0.156883	0.004569	0.017268	0.004647
Fuzzy-PI	0.182720	0.005248	0.019244	0.004657
RBFNN	**0.053051**	**0.001853**	**0.011473**	0.004904

F. Scientific interpretation and limitations

The proposed method performs better for three connected reasons. First, the feedback core preserves conventional error, integral, and filtered-derivative action. Second, the Gaussian RBF layer learns a smooth nonlinear correction rather than a hard switching law. Third, the training target contains load, wind, PV, and parameter-family information, so the network learns a context-dependent correction that can act before the integral state grows substantially.

The numerical comparison also exposes trade-offs. RBFNN generally uses slightly more control effort. The present implementation does not adapt weights online, and its performance therefore depends on whether operation remains reasonably close to the trained domain. Extrapolation beyond the input and parameter ranges should not be assumed safe. These limitations align with broader concerns in verification, safe learning, and neural stability [47]-[52].

Several model limitations must also be stated. The benchmark does not include a full synchronous-machine dq model, boiler-turbine dynamics, network algebraic equations, detailed wind/PV converter controls, transformer saturation, over/under-excitation limiters, measurement noise, communication delay, or protection actions. The renewable profiles are reproducible benchmark inputs rather than site-specific measurements. Consequently, the results support controller comparison on the stated reduced-order voltage channel; they do not certify a real plant or network.

VI. CONCLUSION AND FUTURE WORKS

A renewable-aware RBFNN excitation controller has been developed and compared with PI, filtered PID, and explicit Takagi-Sugeno Fuzzy-PI control for a reduced-order single-area thermal voltage-regulation benchmark with wind and photovoltaic influence. The neural component is genuinely trained inside the supplied MATLAB script from 8000 deterministic samples that cover operating context and a ±25% parameter family. Across the three nominal scenarios, RBFNN reduces IAE relative to PID by 54.2-70.2%. In the severe deterministic perturbed plant, IAE falls by 59.4% and RMS voltage deviation by 53.5%. Over twenty parameter realizations, mean IAE decreases from 0.1569 to 0.0531 p.u.·s. The local linearization built from the actual trained RBF gradient is Hurwitz, and the Lyapunov matrix is positive definite.

Future work should replace the reduced generator-load block with a validated synchronous-machine dq model and a standard excitation system, include detailed converter controls and current limits, and use measured wind, irradiance, and reactive-load data. Robustness should also be tested under measurement noise, delays, limiter activation, topology changes, and out-of-distribution conditions. Hardware-in-the-loop validation and formal reachability or input-to-state stability analysis would be especially valuable before any field-oriented claim is made. Learning-enabled controller verification and neural Lyapunov methods [48], [51], [52] provide promising directions for that next stage.

REFERENCES

[1] N. Hatziargyriou, J. Milanovic, C. Rahmann, V. Ajjarapu, C. Canizares, I. Erlich, D. Hill, I. Hiskens, I. Kamwa, B. Pal, P. Pourbeik, J. J. Sanchez-Gasca, A. M. Stankovic, T. Van Cutsem, V. Vittal, and C. Vournas, "Definition and classification of power system stability - revisited & extended," *IEEE Transactions on Power Systems*, vol. 36, no. 4, pp. 3271-3281, 2021. https://doi.org/10.1109/TPWRS.2020.3041774

[2] IEEE, *IEEE Recommended Practice for Excitation System Models for Power System Stability Studies*, IEEE Std 421.5-2016, 2016. https://doi.org/10.1109/IEEESTD.2016.7553421

[3] IEEE, *IEEE Standard for Interconnection and Interoperability of Distributed Energy Resources with Associated Electric Power Systems Interfaces*, IEEE Std 1547-2018, 2018. https://doi.org/10.1109/IEEESTD.2018.8332112

[4] IEEE, *IEEE Standard for Interconnection and Interoperability of Inverter-Based Resources Interconnecting with Associated Transmission Electric Power Systems*, IEEE Std 2800-2022, 2022. https://doi.org/10.1109/IEEESTD.2022.9762253

[5] J. Machowski, J. W. Bialek, S. Robak, and J. R. Bumby, *Power System Dynamics: Stability and Control*, 3rd ed. Wiley, 2020. https://doi.org/10.1002/9781119526346

[6] Y. Li, Y. Gu, and T. C. Green, "Revisiting grid-forming and grid-following inverters: a duality theory," 2021. https://arxiv.org/abs/2105.13094

[7] F. Milano, F. Dorfler, G. Hug, D. J. Hill, and G. Verbic, "Foundations and challenges of low-inertia systems," in *2018 Power Systems Computation Conference (PSCC)*, 2018. https://doi.org/10.23919/PSCC.2018.8442990

[8] North American Electric Reliability Corporation, *Introductory Guide to Inverter-Based Resources on the Bulk Power System*, 2023. https://www.nerc.com/comm/RSTC_Reliability_Guidelines/White_Paper_Intro_to_IBRs.pdf

[9] ENTSO-E, *High Penetration of Power Electronic Interfaced Power Sources and the Potential Contribution of Grid Forming Converters*, 2020. https://www.entsoe.eu/Documents/Publications/SOC/High_Penetration_of_Power_Electronic_Interfaced_Power_Sources_and_the_Potential_Contribution_of_Grid_Forming_Converters.pdf

[10] B. Kroposki et al., *Research Roadmap on Grid-Forming Inverters*, National Renewable Energy Laboratory, NREL/TP-5D00-73476, 2020. https://www.nrel.gov/docs/fy21osti/73476.pdf

[11] Australian Energy Market Operator, *Application of Advanced Grid-Scale Inverters in the NEM*, 2021. https://aemo.com.au/-/media/files/initiatives/engineering-framework/2021/application-of-advanced-grid-scale-inverters-in-the-nem.pdf

[12] North American Electric Reliability Corporation, *1,200 MW Fault Induced Solar Photovoltaic Resource Interruption Disturbance Report*, 2017. https://www.nerc.com/pa/rrm/ea/1200_MW_Fault_Induced_Solar_Photovoltaic_Resource_/1200_MW_Fault_Induced_Solar_Photovoltaic_Resource_Interruption_Final.pdf

[13] T.-T. Nguyen, T. Vu, S. Paudyal, F. Blaabjerg, and T. L. Vu, "Grid-forming inverter-based wind turbine generators: comprehensive review, comparative analysis, and recommendations," 2022. https://arxiv.org/abs/2203.02105

[14] S. Karagiannopoulos, P. Aristidou, and G. Hug, "Data-driven local control design for active distribution grids using off-line optimal power flow and machine learning techniques," *IEEE Transactions on Smart Grid*, vol. 10, no. 6, pp. 6461-6471, 2019. https://doi.org/10.1109/TSG.2019.2905348

[15] S. Karagiannopoulos, J. Gallmann, M. Gonzalez Vaya, P. Aristidou, and G. Hug, "Active distribution grids offering ancillary services in islanded and grid-connected mode," *IEEE Transactions on Smart Grid*, vol. 11, no. 1, pp. 623-633, 2020. https://doi.org/10.1109/TSG.2019.2927299
[16] H. Xu, A. D. Dominguez-Garcia, V. V. Veeravalli, and P. W. Sauer, "Data-driven voltage regulation in radial power distribution systems," 2019. https://arxiv.org/abs/1901.03173
[17] Y. Chen, Y. Shi, and B. Zhang, "Input convex neural networks for optimal voltage regulation," 2020. https://arxiv.org/abs/2002.08684
[18] Q. Yang, G. Wang, A. Sadeghi, G. B. Giannakis, and J. Sun, "Two-timescale voltage control in distribution grids using deep reinforcement learning," 2019. https://arxiv.org/abs/1904.09374
[19] R. Diao, Z. Wang, D. Shi, Q. Chang, J. Duan, and X. Zhang, "Autonomous voltage control for grid operation using deep reinforcement learning," 2019. https://arxiv.org/abs/1904.10597
[20] S. Mukherjee, R. Huang, Q. Huang, T. L. Vu, and T. Yin, "Scalable voltage control using structure-driven hierarchical deep reinforcement learning," 2021. https://arxiv.org/abs/2102.00077
[21] R. R. Hossain, T. Yin, Y. Du, R. Huang, J. Tan, W. Yu, Y. Liu, and Q. Huang, "Efficient learning of voltage control strategies via model-based deep reinforcement learning," 2022. https://arxiv.org/abs/2212.02715
[22] S. Gupta, A. Mehrizi-Sani, S. Chatzivasileiadis, and V. Kekatos, "Scalable optimal design of incremental Volt/VAR control using deep neural networks," 2023. https://arxiv.org/abs/2301.01440
[23] N. Shi, R. Cheng, L. Liu, Z. Wang, and Q. Zhang, "Data-driven affinely adjustable robust Volt/VAr control," 2022. https://arxiv.org/abs/2209.04598
[24] R. Cheng, N. Shi, S. Maharjan, and Z. Wang, "Automatic self-adaptive local voltage control under limited reactive power," 2022. https://arxiv.org/abs/2206.09269
[25] I. Murzakhanov, S. Gupta, S. Chatzivasileiadis, and V. Kekatos, "Optimal design of Volt/VAR control rules for inverter-interfaced distributed energy resources," 2022. https://arxiv.org/abs/2210.12805
[26] J. Li et al., "Deep reinforcement learning for voltage control and renewable accommodation using spatial-temporal graph information," 2024. https://arxiv.org/abs/2401.15848
[27] D. Arnold et al., "Adaptive control of distributed energy resources for distribution grid voltage stability," 2022. https://arxiv.org/abs/2202.05373
[28] S. Baros, A. Bernstein, and N. Hatziargyriou, "A framework for distributed and compositional stability analysis of power grids," 2020. https://arxiv.org/abs/2003.07475
[29] M. Wang, M. Feng, W. Zhou, and H. Li, "Stabilizing voltage in power distribution networks via multi-agent reinforcement learning with transformer," 2022. https://arxiv.org/abs/2206.03721
[30] M. Golgol and A. Pal, "High-speed voltage control in active distribution systems with smart inverter coordination and deep reinforcement learning," 2023. https://arxiv.org/abs/2311.13080
[31] D. Shi, Q. Zhang, M. Hong, F. Wang, S. Maslennikov, X. Luo, and Y. Chen, "Implementing deep reinforcement learning-based grid voltage control in real-world power systems: challenges and insights," 2024. https://arxiv.org/abs/2410.19880
[32] S. Subedi et al., "Leveraging data-driven models for accurate analysis of grid-tied smart inverters dynamics," 2023. https://arxiv.org/abs/2310.02056
[33] W. Cui, Y. Xie, S. Low, A. Wierman, and B. Zhang, "Leveraging predictions in power system voltage control: an adaptive approach," 2025. https://arxiv.org/abs/2509.09937
[34] G. Ruan, H. Zhong, G. Zhang, Y. He, X. Wang, and T. Pu, "Review of learning-assisted power system optimization," 2020. https://arxiv.org/abs/2007.00210
[35] S. Zhang, Z. Zhu, and Y. Li, "A critical review of data-driven transient stability assessment of power systems: principles, prospects and challenges," 2021. https://arxiv.org/abs/2111.00978
[36] M. Zhang, J. Li, Y. Li, and R. Xu, "Deep learning for short-term voltage stability assessment of power systems," 2021. https://arxiv.org/abs/2102.02526
[37] H. S. Khan, I. S. Mohamed, K. Kauhaniemi, and L. Liu, "Artificial neural network-based voltage control of DC/DC converter for DC microgrid applications," 2021. https://arxiv.org/abs/2111.03207
[38] S. Saadatmand, P. Shamsi, and M. Ferdowsi, "The voltage regulation of a buck converter using a neural network predictive controller," 2020. https://arxiv.org/abs/2002.02544
[39] S. Saadatmand, M. Kavousi, and S. Azizi, "The voltage regulation of boost converters using dual heuristic programming," 2020. https://arxiv.org/abs/2001.10863
[40] S. Saadatmand, M. S. Sanjarinia, P. Shamsi, M. Ferdowsi, and D. C. Wunsch, "Neural network predictive controller for grid-connected virtual synchronous generator," 2019. https://arxiv.org/abs/1908.05199
[41] I. Filip, O. Prostean, C. Vasar, and I. Szeidert, "Adaptive fuzzy controller for synchronous generator," 2018. https://arxiv.org/abs/1803.09543
[42] M. R. H. Mojumder and N. K. Roy, "Review of meta-heuristic optimization algorithms to tune the PID controller parameters for automatic voltage regulator," 2024. https://arxiv.org/abs/2409.00538
[43] A. I. Lakhani, M. A. Chowdhury, and Q. Lu, "Stability-preserving automatic tuning of PID control with reinforcement learning," 2021. https://arxiv.org/abs/2112.15187
[44] I. Goodfellow, Y. Bengio, and A. Courville, *Deep Learning*. MIT Press, 2016. https://www.deeplearningbook.org/
[45] R. S. Sutton and A. G. Barto, *Reinforcement Learning: An Introduction*, 2nd ed. MIT Press, 2018. http://incompleteideas.net/book/the-book-2nd.html
[46] B. Kiumarsi, K. G. Vamvoudakis, H. Modares, and F. L. Lewis, "Optimal and autonomous control using reinforcement learning: a survey," *IEEE Transactions on Neural Networks and Learning Systems*, vol. 29, no. 6, pp. 2042-2061, 2018. https://doi.org/10.1109/TNNLS.2017.2773458
[47] B. Recht, "A tour of reinforcement learning: the view from continuous control," 2018. https://arxiv.org/abs/1806.09460
[48] W. Xiang et al., "Verification for machine learning, autonomy, and neural networks survey," 2018. https://arxiv.org/abs/1810.01989
[49] M. Raissi, P. Perdikaris, and G. E. Karniadakis, "Physics-informed neural networks: a deep learning framework for solving forward and inverse problems involving nonlinear partial differential equations," *Journal of Computational Physics*, vol. 378, pp. 686-707, 2019. https://doi.org/10.1016/j.jcp.2018.10.045
[50] R. T. Q. Chen, Y. Rubanova, J. Bettencourt, and D. Duvenaud, "Neural ordinary differential equations," 2018. https://arxiv.org/abs/1806.07366
[51] Y.-C. Chang, N. Roohi, and S. Gao, "Neural Lyapunov control," 2020. https://arxiv.org/abs/2005.00611
[52] H. Dai, B. Landry, L. Yang, M. Pavone, and R. Tedrake, "Lyapunov-stable neural-network control," 2021. https://arxiv.org/abs/2109.14152